Small polaron dynamics in a two-dimensional magnetic material

Li Yao [1] Aolei Wang [1] Qijing Zheng [1,2,3,*] and Jin Zhao [1,4,3,5,†]

[1] Department of Physics, University of Science and Technology of China, Hefei, Anhui 230026, China
[2] Key Laboratory of Precision and Intelligent Chemistry, University of Science and Technology of China, Hefei, Anhui 230026, China
[3] Hefei National Laboratory, University of Science and Technology of China, Hefei, Anhui 230088, China
[4] ICQD/Hefei National Research Center for Physical Sciences at the Microscale, University of Science and Technology of China, Hefei, Anhui 230026, China
[5] Department of Physics and Astronomy, University of Pittsburgh, Pittsburgh, Pennsylvania 15260, USA

(Received 18 January 2024; revised 5 June 2024; accepted 17 July 2024; published 7 August 2024)

The polaron in magnetic materials can carry not only charge, but also spin information. Therefore, the polaron dynamics in magnetic material is directly correlated with the spin dynamics. In this work, taking two-dimensional (2D) $CoCl_2$ as a prototypical system, it is found that the 2D transition metal dihalide is an ideal platform for small polaron formation. At zero temperature, three distinct structures of small polarons, with their charges mainly localized on one, two, and three Co atoms, have been identified and designated as polarons I, II, and III, respectively. Polarons II and III are stable at 300 K, and their site-to-site hopping involves the transition to each other. Notable in-plane spin canting is observed when polaron II is formed. Moreover, the photoexcited charge carrier lifetime for the spin-minority channel is distinctly reduced by the spin-polarized polaron state in the band gap, making it four orders of magnitude shorter than the spin-majority channel. The existence of a small polaron in 2D magnetic materials provides a different stratagem to design 2D spintronic and polaronic devices.

DOI: 10.1103/PhysRevB.110.054305

I. INTRODUCTION

The idea of the polaron was put forth by Landau and Pekar [1,2], aiming to elucidate the behavior of an electron moving in a dielectric crystal, which involves atoms displacing from their equilibrium positions, forming a phonon cloud and effectively screening the electron's charge. Later, the concept of the polaron was extended to broader domains. Apart from electron-phonon (*e-ph*) coupling, it can be considered that the interaction of fermionic particles with bosonic fields can also give rise to polarons [3,4]. The polarons induced by *e-ph* coupling has been identified in a large variety of materials including transition metal oxides [5–8], alkali halides [9,10], metal halide perovskites [11–14], and organic semiconductors [15,16]. The formation and dynamics of the polaron play a key role in light absorption [17,18], magnetic and spin effects [18], superconductivity [18,19], carrier mobility [20], band-gap modulation [21,22], and so on.

Since the discovery of graphene [23,24], there has been growing interest in the atomically thin two-dimensional (2D) materials due to their rich physical properties and diverse applications [25–27]. The polaron formation in 2D materials has just aroused interest from the research community [3,28–32]. Among 2D materials, manufacturing magnetic 2D nanostructures is particularly interesting for application in spintronics and nanoscale magnetic memory devices [33]. Polaron formation in different 2D magnetic materials were reported very recently [28–30]. Li *et al.* revealed the Jahn-Teller exciton-polaron formation and its dynamics in magnetic semiconductor CrI_3 [30]. More interestingly, very recently two different groups separately reported the creation and manipulation of single small polarons in a monolayer magnetic insulator $CoCl_2$ using scanning tunneling microscopy (STM) back to back [28,29]. The STM measurements were performed at 4 K and density functional theory (DFT) calculations were carried out to understand the structure and electronic properties of small polarons at zero temperature. However, it is not clear if these small polarons are still stable at room temperature. Furthermore, the polaron dynamics is important in many different aspects. If polarons can be easily formed, instead of the free charge, the polaron may play an important role as a charge carrier. Thus, the carrier transport mobility will depend on the site-to-site hopping of small polarons. In addition, the small polaron carries not only a charge, but also a magnetic moment. The dynamics of the small polaron are closely correlated to the charge carrier mobility and the spin dynamics. Therefore, understanding the polaron dynamics in 2D magnetic material such as $CoCl_2$ is of great scientific importance.

This study investigates small polaron dynamics in 2D magnetic materials using first-principles calculations, focusing on $CoCl_2$ as a prototypical system. Three different types of small polarons have been identified through DFT simulations using the hybrid functional at zero temperature, each with distinct local distortions. Moreover, their charge densities mainly localized on one, two, and three Co atoms, hence the notations polarons I, II, and III. Polaron I is unstable at 300 K, quickly transitioning to polaron II. Polarons II and III are stable at 300 K. They can convert to each other by overcoming a 23-meV energy barrier; such polaron transition

*Contact author: zqj@ustc.edu.cn
†Contact author: zhaojin@ustc.edu.cn

is also involved in the polaron hopping process. The polaron dynamics correlates with spin dynamics due to spin-orbit coupling (SOC), exhibiting in-plane spin canting when polaron II forms. The small polaron formation makes the electron-hole (*e-h*) recombination timescale for spin-up and spin-down carriers distinctly different. Spin-polarized polaron states in the band gap enhance *e-h* recombination, reducing excited spin-minority carrier lifetime from 77 ns to 3.3 ps. Conversely, the spin-majority carrier has four orders of magnitude longer lifetime (66 ns), making $CoCl_2$ an ideal system for spin current generation. This work advances the understanding of small polarons dynamics in 2D magnetic materials, offering insight for designing 2D spintronic and polaronic devices.

II. METHOD

We employ DFT calculations with the CP2K package [34,35] and HSE06 functional [36,37] to optimize small polaron structures in a $CoCl_2$ monolayer. A $6 \times 6 \times 1$ supercell with 108 atoms is utilized, and an equilibrium temperature of 300 K is set for polaron dynamics analysis through a 4-ps *ab initio* molecular dynamics (AIMD) simulation using a microcanonical ensemble with 1-fs time step, performed using the HSE06 functional. The photoexcited spin-majority and spin-minority carrier lifetimes are determined using Hefei-NAMD, which combines time-dependent Kohn-Sham equation (TDKS) with the surface hopping scheme based on classical path approximation (CPA) [38–41]. Due to the huge computational cost to include the SOC at the HSE level, magnetic moment orientation is computed via DFT + U with SOC, applying $U = 6.9$ eV [31] to Co 3d orbital in VASP [42–44] with the projector-augmented wave method [45,46]. Additional computational details are provided in the Supplemental Material [47].

III. RESULTS AND DISCUSSIONS

$CoCl_2$ is a magnetic insulator with a band gap of 4.1 eV [48], where the valance band (VB) and conduction band (CB) are dominated by Cl 3p and Co 3d orbitals, respectively (Supplemental Material [47]). The CB is contributed by the spin-down (spin-minority) orbitals. The atomic and band structures and phonon dispersion are shown in Figs. 1(a) and 1(b). The formation of a polaron is related to the electron hopping integral, *e-ph* coupling, and the phonon frequency. A material with large *e-ph* coupling, small electron hopping integral, and low phonon frequency provides suitable conditions for polaron formation [49–51]. The CB of $CoCl_2$ shows very weak dispersion because of the d orbital character, indicating the small electron hopping integral. In addition, it is known that the d orbital is often correlated to strong *e-ph* coupling [52]. Finally, $CoCl_2$ is a relatively "soft" 2D material; the highest longitudinal optical (LO) phonon energy of this material is as low as 36 meV [Figs. 1(i)–1(k)]. As a comparison, in rutile TiO_2, which holds small polarons, the highest LO phonon energy is around 100 meV [53]. Thus, $CoCl_2$ is expected to be a good platform for polaron formation.

By introducing an extra electron into a $(6\times6\times1)$ supercell of $CoCl_2$, three distinct polaron structures (labeled polarons I, II, and III) are observed. The Supplemental Material [47] provides detailed information on determining these polaron structures. Figures 1(c)–1(e) depict the projected density of states (PDOS) and orbital distribution for the three polarons, while Figs. 1(f)–1(h) exhibit the lattice distortion. For each polaron, the range of lattice distortion spans over several unit cells, with the magnitude of the lattice distortion varying between 0.01 and 0.2 Å, characteristic of typical small polarons [4]. More detailed atomic distortion data can be found in Fig. S9 [47]. This lattice distortion stabilizes the additional electron, forming spin-down polaron states in the band gap below the CB. The orbitals of polarons I, II, and III mainly localize on one, two, and three Co atoms, respectively [Figs. 1(c)–1(e)]. Polarons I, II, and III correspond to different local lattice distortions, therefore their DOS are also different as shown in Figs. 1(c)–1(e). Notably, the lattice distortion not only stabilizes states near the CB, forming polaron states, but also localizes and lifts states close to the VB. Polaron I exhibits localized VB states with spin-up polarization, making it a bipolar magnetic semiconductor [54]. In contrast, polarons II and III feature VB states with spin-down polarization, categorizing them as half semiconductors [55]. The binding energies for polarons I, II, and III are 0.221, 0.269, and 0.307 eV, respectively.

As is well known in solid-state physics, the displacements of the atoms in a polaronic lattice distortion can be expressed as a linear combination of different phonons, i.e. [3,56],

$$\Delta\tau_\kappa^P = \frac{2}{\sqrt{N_P}}\sum_q\sum_\upsilon\sqrt{\frac{\hbar}{2M_\kappa\omega_{q\upsilon}}}\epsilon_{q\upsilon}^\kappa B_{q\upsilon}^* e^{iq\cdot R_P}, \quad (1)$$

where $\epsilon_{q\nu}^\kappa$ denotes the orthonormal eigenvector of the νth branch phonon modes with wave vector $\mathbf{q}$ and frequency $\omega_{\mathbf{q}\nu}$. $\mathbf{R}_p$ is the lattice vector of the pth unit cell and M_κ is the mass of the atom κ. The modulus of the quantity $B_{\mathbf{q}\nu}^*$ thus has the physical meaning of the amplitude of the phonon mode $\mathbf{q}\nu$ which contributes to the atomic displacement $\Delta\tau_\kappa^P$. In order to get $B_{\mathbf{q}\nu}^*$, one can perform inverse Fourier transform on Eq. (1) and utilize the orthonormality of $\epsilon_{q\nu}^\kappa$, which leads to

$$B_{\mathbf{q}\nu}^* = \frac{1}{2\sqrt{N_P}}\sum_\kappa\sqrt{\frac{2M_\kappa\omega_{\mathbf{q}\nu}}{\hbar}}\epsilon_{q\nu}^{\kappa *}\cdot\sum_P\Delta\tau_\kappa^P e^{-i\mathbf{q}\cdot\mathbf{R}_p}. \quad (2)$$

Figures 1(i)–1(k) show the phonon dispersion superimposed with $|B_{\mathbf{q}\nu}^*|$ (represented by empty circles with circle sizes proportional to the modulus square of $B_{\mathbf{q}\nu}^*$) for the three polaron states. As can be seen from the figures, the distributions of $|B_{\mathbf{q}\nu}^*|$ for all three polarons reveal a diffusive character in reciprocal space, which is consistent with the localized nature (small polaron) of the lattice distortions in real space. Nevertheless, careful inspections show that there are slight differences between the three polarons. For example, while there are significant contributions from optical phonons in all three polarons, there are fewer contributions from acoustic modes in polaron I, as opposed to polaron II and polaron III.

To form a polaron in 2D $CoCl_2$ monolayer, an excess electron is introduced, which will also induce magnetic moment. The spin density induced by the polaron formation is shown in Fig. S5, which is comparable to the orbital distribution of the polaron state. Moreover, for monolayer

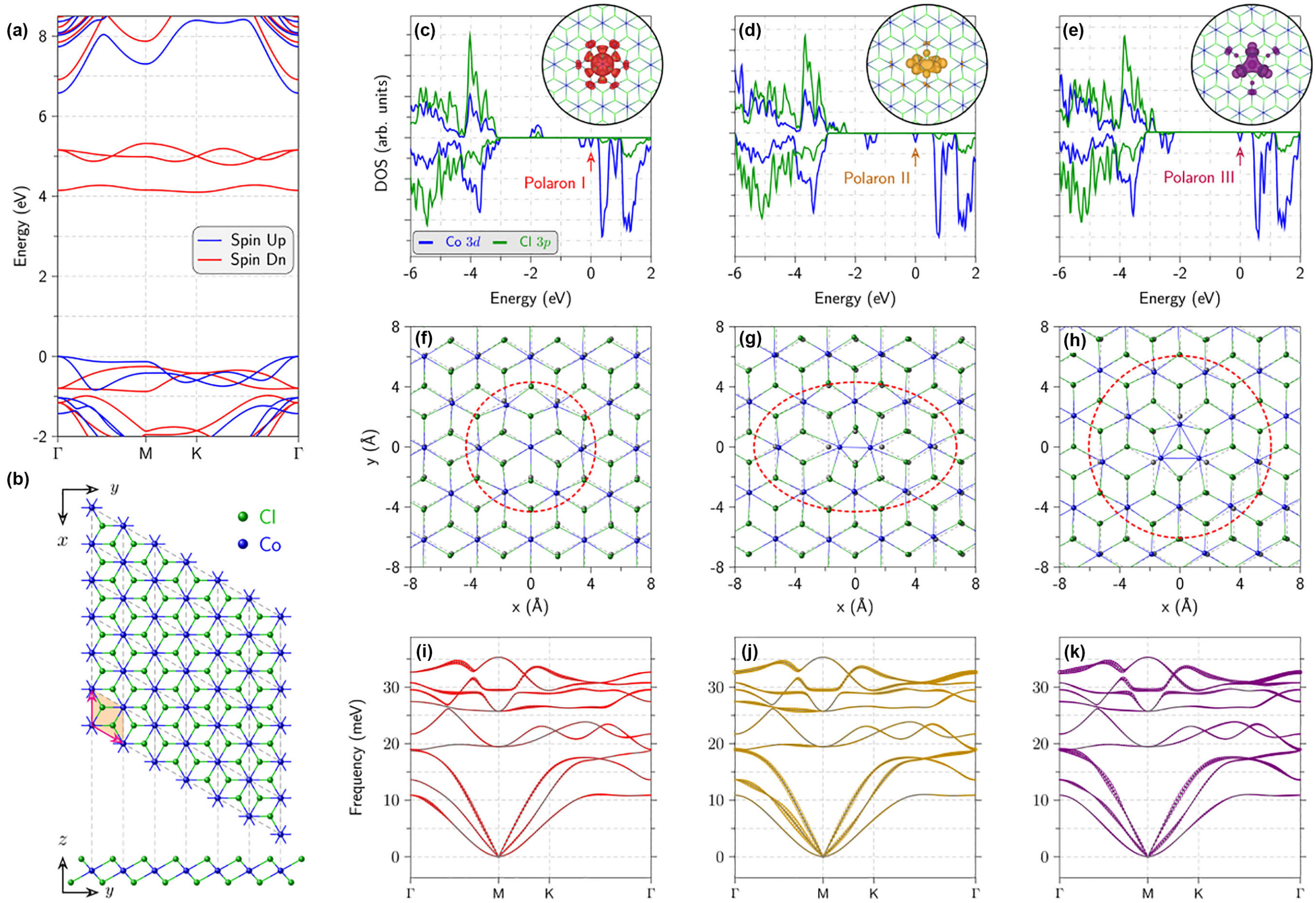

FIG. 1. (a),(b) The band and atomic structures of $CoCl_2$ monolayer. The primitive cell and (6 × 6 × 1) supercell are shown in (b). (c)–(e) Spin-polarized PDOS of the three polaron systems labeled as polarons I, II, and III, respectively. The upper and lower lines represent the spin-up and spin-down components of the PDOS. The reference energy is the highest occupied electronic state. The orbital distributions of the three polaron states are plotted in the solid circles, with red, yellow, and purple color. (f)–(h) Top views of structure distortion of the polarons I, II, and III, respectively. The dashed circles indicate regions where the lattice shows notable distortion. The lattice distortion is magnified threefold to make it clear for readers. Green and blue balls represent Co and Cl atoms in the polaron structure, respectively, while the gray balls represent the pristine atomic structure of $CoCl_2$. The average elongation of the Co-Cl bond around distorted Co atom is 0.053, 0.046, and 0.034 Å for polarons I, II, and III, respectively. (i)–(k) Normal mode decomposition of the polaron induced lattice distortion. The phonon dispersions are superimposed with $|B^*_{\mathbf{q}\nu}|^2$, which are represented with empty circles with the size of the circles proportional to $|B^*_{\mathbf{q}\nu}|^2$.

$CoCl_2$, a ferromagnetic insulator with sizable magnetocrystalline anisotropies exhibits magnetic properties influenced by SOC [57,58]. Formation of a polaron is expected to change the orbital distribution and impact the magnetic structure through SOC. In Fig. 2, we illustrate the orientation of in-plane and out-of-plane magnetic moments for pristine $CoCl_2$ and $CoCl_2$ with three small polarons. Polaron III has negligible impact on the magnetic structure, while polaron I results in a slightly reduced magnetic moment with almost no change in direction. The most pronounced effect on the magnetic structure is observed in polaron II, as evidenced by spin canting on the two Co atoms where the polaron localizes. The magnetic moments of the two Co atoms rotates approximately 21° and 11° in the 2D $CoCl_2$ plane, respectively, and their magnitudes are reduced by around 0.01 μ_B and 0.7 μ_B, respectively [Fig. 2(c)]. In the out-of-plane direction [Fig. 2(g)], one magnetic moment increases by $0.35\mu_B$ and the other decreases by $0.36\mu_B$.

Since a polaron is more stable than a free charge carrier in $CoCl_2$, the charge transfer properties in $CoCl_2$ are closely correlated with the polaron dynamics. Moreover, since polaron formation influences the spin structure, the polaron dynamics is also directly related to the spin dynamics. Our investigation focuses on polaron dynamics at 300 K. The localization of the polaron states can be numerically quantified using the inverse participation ratio (IPR) [59–61]. For a wave function ϕ, e.g., represented on a 3D grid, the IPR can be evaluated as [59]

$$\mathrm{IPR}(\phi) = \frac{\sum_{n=1}^{N} |\phi(n)|^4}{\left[\sum_{n=1}^{N} |\phi(n)|^2\right]^2}, \tag{3}$$

where n is the index for the grid and $\phi(n)$ is the value of the wave function on the grid. For a totally delocalized state, i.e., a homogeneous wave function, the values of the wave function at all the grid points are the same, hence IPR $= 1/N$. On the other hand, if the wave function is a totally localized one, for example delta-function-like, then the values of the wave function are nonzero only at one grid point, and as a result IPR $= 1.0$. For a general wave function, the IPR falls

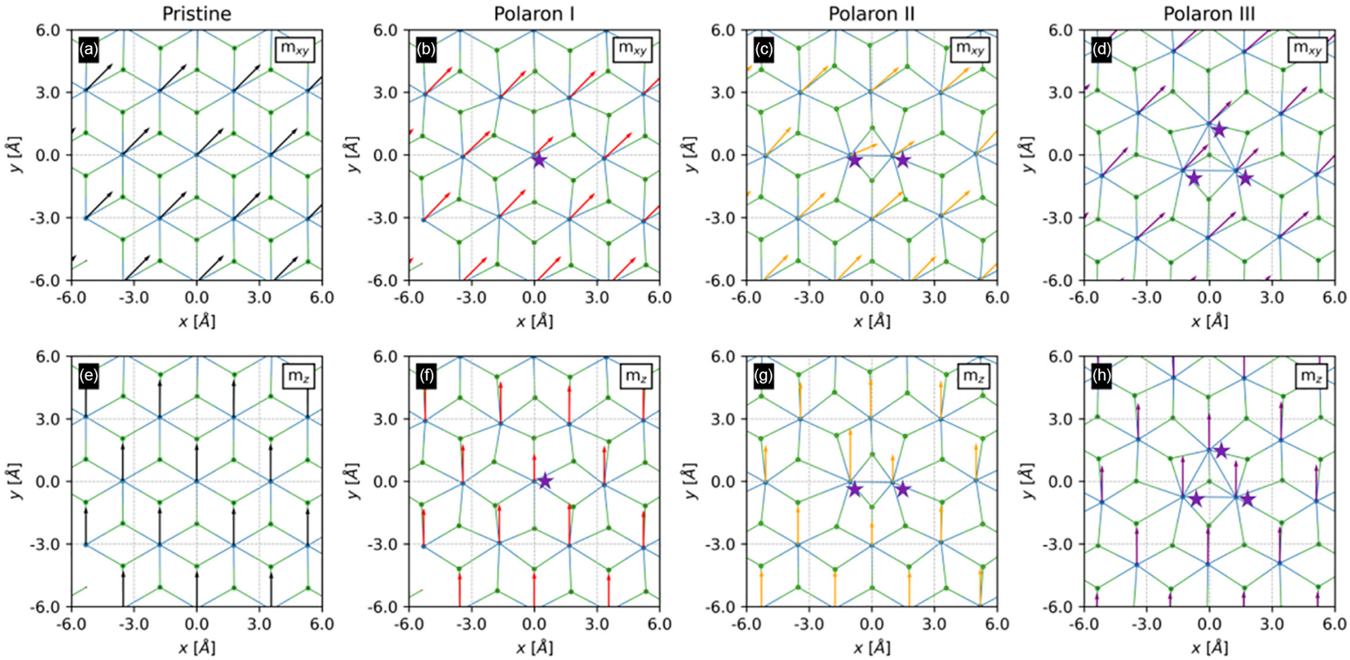

FIG. 2. Magnetic structure change induced by polaron formation. The direction and magnitude of the magnetic moment on each Co atom are indicated by the arrows. The in-plane and out-of-plane components of the magnetic moments are shown (a)–(d) and (e)–(h), respectively. The black and gray arrows in (a)–(h) represent the magnetic moments in pristine $CoCl_2$ without polaron formation. The in-plane and out-of-plane magnetic moments are 1.64 μ_B and 1.58 μ_B, respectively. The arrows in (b)–(d) and (f)–(h) represent the magnetic moments with the polaron formation. The violet stars indicate the position of the Co atoms where the extra charge of the polaron localizes.

between [$1/N$, 1.0]. If the number of grid points is very large, the IPR ranges approximately from 0 to 1, where a smaller IPR indicates a more delocalized state.

We traced the evolution of the polaron states, as can be seen by the green solid line in Fig. 3(a), where we also show IPRs of the three polaron states at 0 K with dashed lines. Following the equilibration, we introduce an extra electron at $ta = 0$ fs. Polaron I is formed within the first 90 fs, as is consistent with the sharp increase in IPR. This process aligns with a half period of the A_{1g} optical phonon mode. However, polaron I quickly transforms into polaron III by $t = 150$ fs, as observed in the polaron charge density snapshots. Subsequently, polarons II and III exhibit mutual transitions or site hopping, while polaron I only occasionally appears transiently during transition or hopping processes. For instance, around $t = 2700$ fs, when polaron III hops from one site to another, polaron I emerges temporarily as an intermediate product. Figure 3(b) displays the histogram of the IPR in Fig. 3(a), revealing distinct peaks for polarons II and III.

To elucidate the dynamic behavior of small polarons in $CoCl_2$, we calculated transition and hopping barriers among polarons I, II, and III [Figs. 3(c)–3(f)]. Here, "transition" is defined as the conversion between different types of small polarons, while "hopping" represents the movement of the same type of small polaron from one position to another. Notably, the transition barrier from polaron I to II is only 3.4 meV, explaining its instability at 300 K. The polaron II to polaron III transition has a barrier of 23 meV, while the reverse is 77 meV, facilitating easy observation of their interconversion at 300 K. Polarons II and III exhibit site-to-site hopping, occurring directly or indirectly via their transition. Calculations reveal direct hopping barriers of 28 and 100 meV for polarons II and III, respectively, larger than the transition barriers between polarons II and III. Hence, we propose that small polaron hopping in $CoCl_2$ involves transitions between polarons II and III.

The polaron dynamics simulation indicates that only polarons II and III are stable at 300 K. Moreover, the DOS of polarons II and III shown in Figs. 1(d) and 1(e) indicate that the formation of polarons II and III reduce the band gap of spin-down electronic states distinctly, making the $CoCl_2$ system a half semiconductor. For a half semiconductor, the band gap sizes for spin-up and spin-down states differ, potentially resulting in different lifetimes of spin-up and spin-down excited carriers. To confirm this point, we use *ab initio* NAMD to study the lifetimes of spin-up and spin-down excited carriers, and the results are shown in Fig. 4.

Figures 4(a) and 4(b) show the time evolution of the electronic states for pristine $CoCl_2$ obtained by AIMD at 300 K. The averaged energy band gaps for the spin-up and spin-down states are 5.97 and 3.45 eV, respectively. The lifetime for the excited hole to recombine with the excited electron are calculated to be 9.0 and 77.0 ns for spin-up and spin-down states, respectively as shown in Figs. 4(c) and 4(d). The factors affecting the excited carrier lifetime include the size of the band gap, the orbital overlap between the CBM and VBM, and the strength of their coupling with phonons. Here, the lifetime of spin-up excited carriers is shorter by an order of magnitude compared to spin-down excited carriers. This can be understood by examining the DOS and orbital distributions depicted in Fig. S8 for pristine $CoCl_2$. For spin-down electron states, both the CBM and VBM are primarily contributed by Co_3*d* orbitals. The localized character of *d* orbitals results in a small overlap between the CBM and VBM. In contrast, for

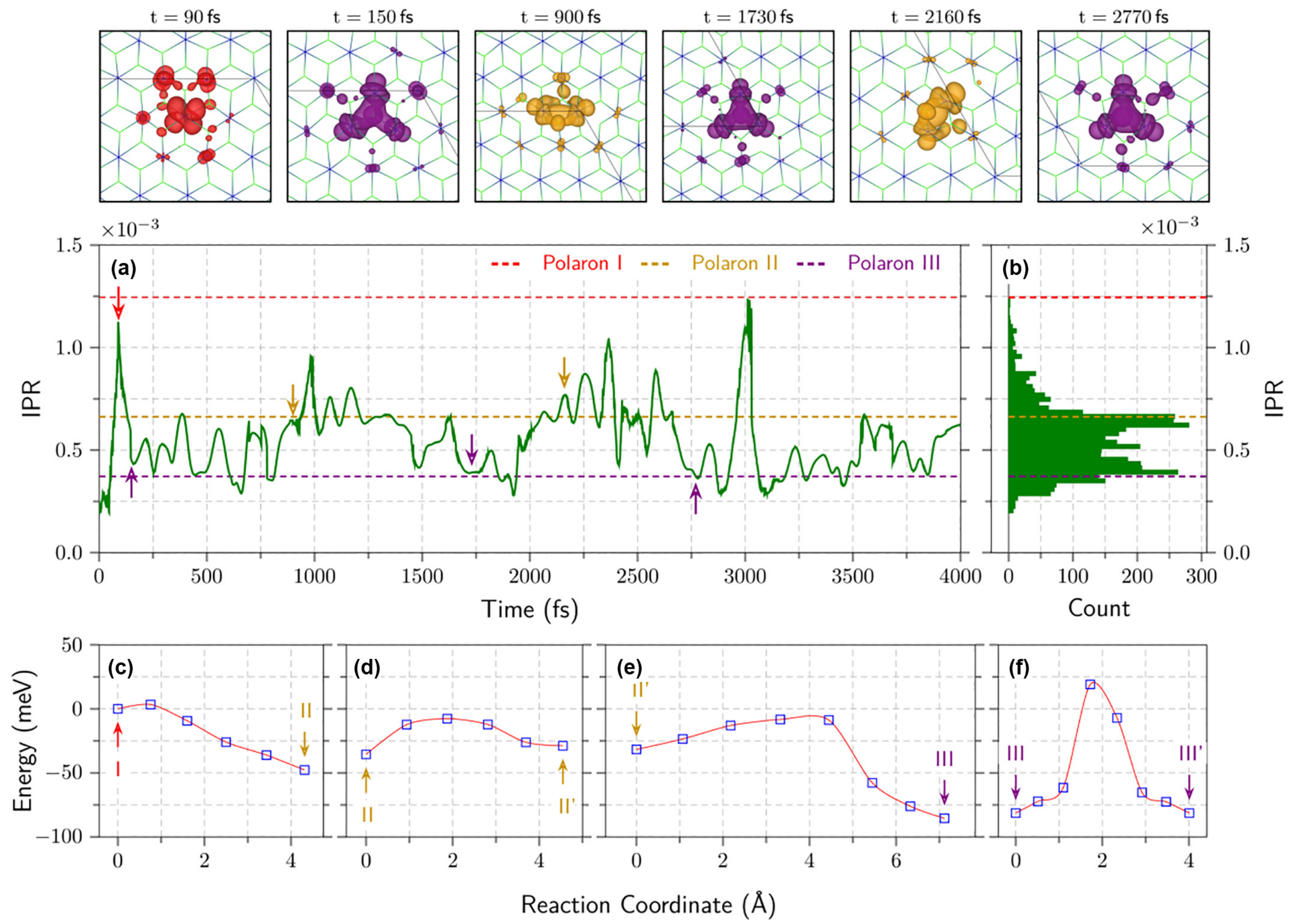

FIG. 3. (a) The time evolution of IPR of the polaron state during 4 ps AIMD simulation with snapshots of the polaron state distribution. (b) The histogram of the IPR in (a). The red, yellow, and purple dashed lines indicate the IPR of polarons I, II, and III at 0 K, respectively. (c)–(f) Transition and hopping barriers among different polarons.

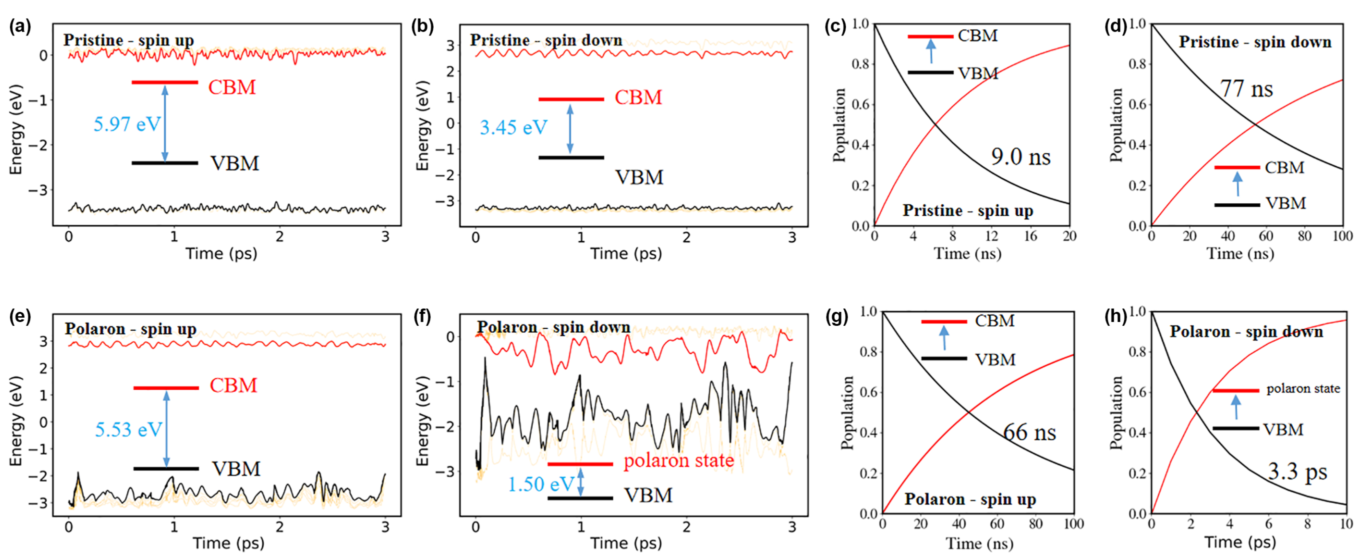

FIG. 4. (a),(b) Time-dependent energy evolution for spin-up and spin-down electronic states in pristine $CoCl_2$ during the AIMD simulation. The energy reference is the highest occupied spin down state at $t = 0$ fs. The average energy band gaps for the spin-up and spin-down states are 5.97 and 3.45 eV, respectively. (c),(d) Time-dependent excited hole population for the spin-up and spin-down states in pristine $CoCl_2$. (e),(f) Time-dependent energy evolution for spin-up and spin-down electronic states in $CoCl_2$ with polaron formation during the AIMD simulation. The energy reference is the highest occupied spin down state at $t = 0$ fs. The average spin-down band gap between the VBM and the polaron state is 1.50 eV, and the average spin-up band gap between the VBM and the CBM is 5.53 eV. (g),(h) Time-dependent hole population for the spin-up and spin-down states in $CoCl_2$ with polaron.

spin-up states, there is a significant contribution from Cl_3p orbitals in both the CBM and VBM. Consequently, the overlap between them is relatively large, leading to a shorter lifetime for spin-up excited carriers.

After the polaron is generated by an excess electron, the time evolution of spin-up and spin-down electronic states are shown in Figs. 4(e) and 4(f). First, the energy band gap of the spin-down electronic states is distinctly reduced by the polaron state in the band gap. The averaged spin-down band gap is calculated to be 1.5 eV. Furthermore, the polaron state and the VBM states exhibit pronounced energy oscillations, indicating strong *e-ph* coupling. The reduction of band gap and enhanced *e-ph* coupling suppress the excited carrier lifetime from 77.0 ns to 3.3 ps. In contrast, for spin-up states, the polaron formation resulting in local distortions reduces the orbital overlap between the CBM and VBM (see Fig. S8). Interestingly, this increases the spin-up carrier lifetime from 9 to 66 ns. As a result, the excited carrier lifetime for spin-up and spin-down states differs by four orders of magnitude. When *e-h* pairs are excited by photons, nearly equal numbers of spin-up and spin-down *e-h* pairs will be generated. Here, it is expected the spin-down *e-h* pairs recombine on 3.3 ps, leaving only the spin-up *e-h* pairs, which have a much longer lifetime. The residual electrons and holes are both spin polarized and enable the formation of spin-polarized current.

The existence of polarons I and III was certified by the STM measurements [28]. However, polaron II was not directly observed in the experiments. This may be due to the fact that $CoCl_2$ in the STM measurements is not a free-standing monolayer but is placed on a substrate. The interlayer interaction may affect the relative stability of different small polarons. Graphite was used in the STM measurement in the work by Liu *et al.*, which has threefold rotational symmetry [28]. This might be the reason that polarons I and III, which also have threefold rotational symmetry, are easy to observe.

The dynamics aspects of the small polaron in $CoCl_2$ are expected to be detectable by different experimental techniques. Liu *et al.* observed the hopping of the polarons in $CoCl_2$ under tip perturbation, often occurring during STM scanning [28]. The atomic magnetic structure can be measured by spin-polarized STM. For example, Miao *et al.* identified the existence of a spin spiral state with canted plane in monolayer NiI_2 [32]. Therefore, the spin dynamics correlated with the polaron dynamics is expected to be detectable by the spin-polarized STM. Finally, the excited carrier lifetime can be detected by the ultrafast time-resolved transient spin-polarized photoluminescence and photoabsorption spectra [62].

Each optimized polaron structure corresponds to a local energy minimum. Therefore, the number of small polaronic structures is actually determined by the potential energy surface of the system, which is rather difficult to estimate when the atomic structure is complex. In this work, we use the approach described in the Supplemental Material to find the polaron structures. In fact, we are not assuring that we have found all the small polaron structures at zero temperature. Using global search methods, such as genetic algorithms, may lead to the discovery of additional small polaron structures.

Small polarons are not only identified in $CoCl_2$ but also in other transition metal dihalides like NiI_2 [32] and $FeCl_2$ [29]. We suggest that the prevalence of small hopping integral, low phonon energy, and substantial electron-phonon interaction in these materials establishes an ideal platform for polaron formation and manipulation. These materials, known for their diverse magnetic properties [57,63,64], position polarons as not just charge carriers but also single spin carriers. The interplay of polaron dynamics with the magnetism of transition metal dihalides holds significant promise for applications in spintronics and data storage.

ACKNOWLEDGMENTS

J.Z. acknowledges the support of Innovation Program for Quantum Science and Technology 2021ZD0303306, Strategic Priority Research Program of the Chinese Academy of Sciences, Grant No. XDB0450101; NSFC, Grants No. 12125408 and No. 12334004. Q.Z. acknowledges the support of the National Natural Science Foundation of China (NSFC), Grant No. 12174363. Calculations were performed at Hefei Advanced Computing Center, Supercomputing Center at USTC and Beijing Super Cloud Center (BSCC [65]).

[1] L. D. Landau, Electron motion in crystal lattices, Phys. Z. Sowjetunion **3**, 664 (1933).
[2] S. I. Pekar, Local quantum states of electrons in an ideal ion crystal, Zh. Eksp. Teor. Phys. **16**, 341 (1946).
[3] W. H. Sio and F. Giustino, Polarons in two-dimensional atomic crystals, Nat. Phys. **19**, 629 (2023).
[4] C. Franchini, G. Kresse, and R. Podloucky, Polarons in materials, Phys. Rev. Lett. **102**, 256402 (2009).
[5] M. Reticcioli, U. Diebold, G. Kresse, and C. Franchini, Small polarons in transition metal oxides, in *Handbook of Materials Modeling*, edited by W. Andreoni and S. Yip (Springer, Cham, 2020), pp. 1035–1073.
[6] P. Nagels, M. Denayer, and J. Devreese, Electrical properties of single crystals of uranium dioxide, Solid State Commun. **1**, 35 (1963).
[7] C. Cheng, Y. Zhu, W.-H. Fang, R. Long, and O. V. Perzhdo, CO adsorbate promotes polaron photoactivity on the reduced rutile TiO_2(110) surface, JACS Au **1**, 550 (2022).
[8] C. Cheng, Y. Zhu, Z. Zhou, R. long, and W. Fang, Photoinduced small electron polarons generation and recombination in hematite, npj Comput. Mater. **8**, 148 (2022).
[9] X.-J. Ma, W. Zhang, S. Han, Xiangliang, P.-F. Li, C.-L. Zhao, Z.-H. Ding, Y. Sun, and J.-L. Xiao, The level-splitting effects of spin-orbit interaction on strong-coupling polaron in quantum dots with alkali halide, Physica E **144**, 115387 (2022).
[10] A. S. Tygesen, J. H. Chang, and J. M. García-Lastra, Dependence of polaron migration barriers on the fraction of Fock exchange in hybrid functionals: A systematic study of V_k centers in alkali halides, Phys. Rev. B **108**, 045120 (2023).

[11] K. Miyata, D. Meggiolaro, M. T. Trinh, P. P. Joshi, E. Mosconi, S. C. Jones, F. D. Angelis, and X.-Y. Zhu, Large polarons in lead halide perovskites, Sci. Adv. **3**, e1701217 (2017).

[12] D. Cortecchia, J. Yin, A. Bruno, S.-Z. A. Lo, G. G. Gurzadyan, S. Mhaisalkar, J.-L. Brédas, and C. Soci, Polaron self-localization in white-light emitting hybrid perovskites, J. Mater. Chem. C **5**, 2771 (2017).

[13] H. Lu and R. long, Photoinduced small hole polarons formation and recombination in all-inorganic perovskite from quantum dynamics simulation, J. Phys. Chem. Lett. **13**, 7532 (2022).

[14] F. Wang, Y. Fu, M. E. Ziffer, Y. Dai, S. F. Maehrlein, and X.-Y. Zhu, Solvated electrons in solids ferroelectric large polarons in lead halide perovskites, J. Am. Chem. Soc. **143**, 5 (2021).

[15] A. Zhugayevych and S. Tretiak, Theoretical description of structural and electronic properties of organic photovoltaic materials, Annu. Rev. Phys. Chem. **66**, 305 (2015).

[16] V. Coropceanu, J. Cornil, D. Filho, Y. Olivier, R. Silbey, and J. Brédas, Charge transport in organic semiconductors, Chem. Rev. **107**, 926 (2007).

[17] J. V. Nguepnang, C. Kenfack-Sadem, A. Kenfack-Jiotsa, C. Guimapi, A. J. Fotue, and A. E. Merad, Electron–phonon coupling contribution on the optical absorption and the dynamic of exciton-polaron in monolayer transition metal dichalcogenides, Opt. Quantum Electron. **53**, 654 (2021).

[18] A. S. Alexandrov, *Polarons in Advanced Materials* (Springer, Dordrecht, 2008), Vol. 103.

[19] M. Kang, S. W. Jung, W. J. Shin, Y. Sohn, S. H. Ryu, T. K. Kim, M. Hoesch, and K. S. Kim, Holstein polaron in a valley-degenerate two-dimensional semiconductor, Nat. Mater. **17**, 676 (2018).

[20] I. N. Hulea, S. Fratini, H. Xie, C. L. Mulder, N. N. Iossad, G. Rastelli, S. Ciuchi, and A. F. Morpurgo, Tunable Fröhlich polarons in organic single-crystal transistors, Nat. Mater. **5**, 982 (2006).

[21] Y. Xiao, Z.-Q. Li, and Z.-W. Wang, Polaron effect on the bandgap modulation in monolayer transition metal dichalcogenides, J. Phys.: Condens. Matter **29**, 485001 (2017).

[22] F. Zheng and L.-W. Wang, Large polaron formation and its effect on electron transport in hybrid perovskites, Energy Environ. Sci. **12**, 1219 (2019).

[23] K. S. Novoselov, A. K. Geim, S. V. Morozov, D. Jiang, Y. Zhang, S. V. Dubonos, I. V. Grigorieva, and A. A. Firsov, Electric field effect in atomically thin carbon films, Science **306**, 666 (2004).

[24] K. S. Novoselov, A. K. Geim, S. V. Morozov, D. Jiang, M. I. Katsnelson, I. V. Grigorieva, S. V. Dubonos, and A. A. Firsov, Two-dimensional gas of massless Dirac fermions in graphene, Nature (London) **438**, 197 (2005).

[25] K. F. Mak and J. Shan, Photonics and optoelectronics of 2D semiconductor transition metal dichalcogenides, Nat. Photonics **10**, 216 (2016).

[26] B. Luo, G. Liu, and L. Wang, Recent advances in 2D materials for photocatalysis, Nanoscale **8**, 6904 (2016).

[27] C. Robert, D. Lagarde, F. Cadiz, G. Wang, B. Lassagne, T. Amand, A. Balocchi, P. Renucci, S. Tongay, B. Urbaszek *et al.*, Exciton radiative lifetime in transition metal dichalcogenide monolayers, Phys. Rev. B **93**, 205423 (2016).

[28] H. Liu, A. Wang, P. Zhang, C. Ma, C. Chen, Z. Liu, Y.-Q. Zhang, B. Feng, P. Cheng, J. Zhao *et al.*, Atomic-scale manipulation of single-polaron in a two-dimensional semiconductor, Nat. Commun. **14**, 3690 (2023).

[29] M. Cai, M. Miao, Y. Liang, Z. Jiang, Z.-Y. Liu, W.-H. Zhang, X. Liao, L.-F. Zhu, D. West, S. Zhang *et al.*, Manipulating single excess electrons in monolayer transition metal dihalide, Nat. Commun. **14**, 3691 (2023).

[30] X. Li, A. Wang, H. Chen W. Tao, Z. Chen, C. Zhang, Y. Li, Y. Zhang, H. Shang, Y.-X. Weng *et al.*, Ultrafast spontaneous localization of a Jahn-Teller exciton polaron in two-dimensional semiconducting CrI_3 by symmetry breaking, Nano Lett. **22**, 8755 (2022).

[31] Y. Liang, M. Cai, L. Peng, Z. Jiang, D. West, Y.-S. Fu, and S. Zhang, Small polaron formation by electron-electron interaction, arXiv:2110.01790.

[32] M. Miao, N. Liu, W. Zhang, D. Wang, W. Ji, and Y.-S. Fu, Spin-resolved imaging of atomic-scale helimagnetism in monolayer NiI_2, arXiv:2309.16526.

[33] W. Han, R. K. Kawakami, M. Gmitra, and J. Fabian, Graphene spintronics, Nat. Nanotechnol. **9**, 794 (2014).

[34] J. Hutter, M. Iannuzzi, F. Schiffmann, and J. VandeVondele, CP2K: Atomistic simulations of condensed matter systems, Comput. Mol. Sci. **4**, 15 (2014).

[35] T. D. Kühne, M. Iannuzzi, M. D. Ben, V. V. Rybkin, P. Seewald, F. Stein, T. Laino, R. Z. Khaliullin,O. Schütt, F. Schiffmann *et al.*, CP2K: An electronic structure and molecular dynamics software package-Quickstep: Efficient and accurate electronic structure calculations, J. Chem. Phys. **152**, 194103 (2020).

[36] J. Heyd and G. E. Scuseria, Assessment and validation of a screened Coulomb hybrid density functional, J. Chem. Phys. **120**, 7274 (2004).

[37] A. V. Krukau, O. A. Vydrov, A. F. Izmaylov, and G. E. Scuseria, Influence of the exchange screening parameter on the performance of screened hybrid functionals, J. Chem. Phys. **125**, 224106 (2006).

[38] Q. Zheng, W. Chu, C. Zhao, L. Zhang, H. Guo, Y. Wang, X. Jiang, and J. Zhao, *Ab initio* nonadiabatic molecular dynamics investigations on the excited carriers in condensed matter systems, WIREs Comput. Mol. Sci. **9**, e1411 (2019).

[39] L. Wang, A. Akimov, and O. V. Prezhdo, Recent progress in surface hopping: 2011–2015, J. Phys. Chem. Lett. **7**, 2100 (2016).

[40] A. V. Akimov and O. V. Prezhdo, The PYXAID program for non-adiabatic molecular dynamics in condensed matter systems, J. Chem. Theory Comput. **9**, 4959 (2013).

[41] C. F. Craig, W. R. Duncan, and O. V. Prezhdo, Trajectory surface hopping in the time-dependent Kohn-Sham approach for rlectron-nuclear fynamics, Phys. Rev. Lett. **95**, 163001 (2005).

[42] G. Kresse and J. Furthmüller, Efficient iterative schemes for *ab initio* total-energy calculations using a plane-wave basis set, Phys. Rev. B **54**, 11169 (1996).

[43] G. Kresse and J. Furthmüller, Efficiency of ab-initio total energy calculations for metals and semiconductors using a plane-wave basis set, Comput. Mater. Sci. **6**, 15 (1996).

[44] G. Kresse and J. Hafner, *Ab initio* molecular dynamics for open-shell transition metals, Phys. Rev. B **48**, 13115 (1993).

[45] G. Kresse and D. Joubert, From ultrasoft pseudopotentials to the projector augmented-wave method, Phys. Rev. B **59**, 1758 (1999).

[46] P. E. Blöchl, Projector augmented-wave method, Phys. Rev. B **50**, 17953 (1994).

[47] See Supplemental Material at http://link.aps.org/supplemental/10.1103/PhysRevB.110.054305 for additional calculation details, calculation results, and discussion, which includes Refs. [38,42–44,66–77].

[48] V. V. Kulish and W. Huang, Single-layer metal halides MX_2 (X = Cl, Br, I): Stability and tunable magnetism from first principles and Monte Carlo simulations, J. Mater. Chem. C **5**, 8734 (2017).

[49] M. Capone, W. Stephan, and M. Grilli, Small-polaron formation and optical absorption in Su-Schrieffer-Heeger and Holstein models, Phys. Rev. B **56**, 4484 (1997).

[50] C. A. Perroni, E. Piegari, M. Capone, and V. Cataudella, Polaron formation for nonlocal electron-phonon coupling: A variational wave-function study, Phys. Rev. B **69**, 174301 (2024).

[51] G. Wellein, H. Röder, and H. Fehske, Polarons and bipolarons in strongly interacting electron-phonon systems, Phys. Rev. B **53**, 9666 (1996).

[52] J. J. Zhou, J. Park, I. Timrov, A. Floris, M. Cococcioni, N. Marzari, and M. Bernardi, *Ab initio* electron-phonon interactions in correlated electron systems, Phys. Rev. Lett. **127**, 126404 (2021).

[53] B. Wehinger, A. Bosak, and P. T. Jochym, Soft phonon modes in rutile TiO_2, Phys. Rev. B **93**, 014303 (2016).

[54] J. Li, X. Li, and J. Yang, A review of bipolar magnetic semiconductors from theoretical aspects, Fundam. Res. **2**, 511 (2022).

[55] X. Wu, J. Han, Y. Feng, G. Li, C. Wang, G. Ding, and G. Gao, Half-metals and half-semiconductors in a transition metal doped $SnSe_2$ monolayer: A first-principles study, RSC Adv. **7**, 44499 (2017).

[56] W. H. Sio, C. Verdi, S. Poncé, and F. Giustino, *Ab initio* theory of polarons: Formalism and applications, Phys. Rev. B **99**, 235139 (2019).

[57] A. S. Botana and M. R. Norman, Electronic structure and magnetism of transition metal dihalides: Bulk to monolayer, Phys. Rev. Mater. **3**, 044001 (2019).

[58] J. Y. Ni, X. Y. Li, D. Amoroso, X. He, J. S. Feng, E. J. Kan, S. Picozzi, and H. J. Xiang, Giant biquadratic exchange in 2D magnets and its role in stabilizing ferromagnetism of $NiCl_2$ monolayers, Phys. Rev. Lett. **127**, 247204 (2021).

[59] S. Ganeshan, J. H. Pixley, and S. Das Sarma, Nearest neighbor tight binding models with an exact mobility edge in one dimension, Phys. Rev. Lett. **114**, 146601 (2015).

[60] P. Frey, D. Mikhail, S. Rachel, and L. Hackl, Probing Hilbert space fragmentation and the block inverse participation ratio, Phys. Rev. B **109**, 064302 (2024).

[61] L. E. Hintzsche, C. M. Fang, T. Watts, M. Marsman, G. Jordan, M. W. P. E. Lamers, A. W. Weeber, and G. Kresse, Density functional theory study of the structural and electronic properties of amorphous silicon nitrides: Si_3N_{4-x}:H, Phys. Rev. B **86**, 235204 (2012).

[62] D. Zhang, Y. Liu, M. He, A. Zhang, S. Chen, Q. Tong, L. Huang, Z. Zhou, W. Zheng, M. Chen *et al.*, Room temperature near unity spin polarization in 2D Van der Waals heterostructures, Nat. Commun. **11**, 4442 (2020).

[63] M. A. McGuire, Crystal and magnetic structures in layered, transition metal dihalides and trihalides, Crystals **7**, 121 (2017).

[64] X. Li, Z. Zhang, and H. Zhang, High throughput study on magnetic ground states with Hubbard U corrections in transition metal dihalide monolayers, Nanoscale Adv. **2**, 495 (2020).

[65] http://www.blsc.cn/.

[66] J. VandeVondele, M. Krack, F. Mohamed, M. Parrinello, T. Chassaing, and J. Hutter, QUIKSTEP: Fast and accurate density functional calculations using a mixed Gaussian and plane waves approach, Comput. Phys. Commun. **167**, 103 (2005).

[67] G. Lippert, J. Hutter, and M. Parrinello, The Gaussian and augmented-plane-wave density functional method for *ab initio* molecular dynamics simulations, Theor. Chem. Acc. **103**, 124 (1999).

[68] S. Goedecker, M. Teter, and J. Hutter, Separable dual-space Gaussian pseudopotentials, Phys. Rev. B **54**, 1703 (1996).

[69] J. V. Vondele and J. Hutter, Gaussian basis sets for accurate calculations on molecular systems in gas and condensed phases, J. Chem. Phys. **127**, 114105 (2007).

[70] M. Guidon, J. Hutter, and J. V. Vondele, Auxiliary density matrix methods for Hartree-Fock exchange calculations, J. Chem. Theory Comput. **6**, 2348 (2010).

[71] G. Henkelman, B. P. Uberuaga, and H. Jónsson, A climbing image nudged elastic band method for finding saddle points and minimum energy paths, J. Chem. Phys. **113**, 9901 (2000).

[72] S. L. Dudarev, G. A. Botton, S. Y. Savrasov, C. J. Humphreys, and A. P. Sutton, Electron-energy-loss spectra and the structural stability of nickel oxide: An LSDA+U study, Phys. Rev. B **57**, 1505 (1998).

[73] S. A. Tolba, K. M. Gameel, B. A. Ali, H. A. Almossalami, and N. K. Allam, in *Density Functional Calculations - Recent Progresses of Theory and Application*, edited by G. Yang (BoD – Books on Demand, 2018).

[74] B. Himmetoglu, A. Floris, S. D. Gironcoli, and M. Cococcioni, Hubbard-corrected DFT energy functionals: The LDA+U description of correlated systems, Int. J. Quantum Chem. **114**, 14 (2014).

[75] A. Togo, First-principles phonon calculations with phonopy and phono3py, J. Phys. Soc. Jpn. **92**, 012001 (2023).

[76] A. Togo, L. Chaput, T. Tadano, and I. Tanaka, Implementation strategies in phonopy and phono3py, J. Phys.: Condens. Matter **35**, 353001 (2023).

[77] L. Li, R. Long, T. Bertolini, and O. V. Prezhdo, Sulfur adatom and vacancy accelerate charge recombination in MoS_2 but by different mechanisms: Time-domain *ab initio* analysis, Nano Lett. **17**, 7962 (2017).